Macromolecules
ARTICLE

Macromolecules **2011**, *44*, 757–766 **757**
DOI: 10.1021/ma1025362

Self-Assembled Superlattices of Polyamines in a Columnar Liquid Crystal

Carel F.C. Fitié,[†] Eduardo Mendes,[‡] Mark A. Hempenius,[§] and Rint P. Sijbesma*[,†]

[†]*Laboratory of Macromolecular and Organic Chemistry, Eindhoven University of Technology, P.O. Box 513, 5600 MB Eindhoven, The Netherlands,* [‡]*Section NanoStructured Materials, Department of Chemical Engineering, Delft University of Technology, Julianalaan 136, 2628BL Delft, The Netherlands, and* [§]*Faculty of Science and Technology, MESA+ Institute for Nanotechnology, University of Twente, P.O. Box 217, 7500 AE Enschede, The Netherlands*

Received November 7, 2010; Revised Manuscript Received December 17, 2010

ABSTRACT: We show that the principle of orthogonal self-assembly, which makes use of mutually noninterfering interactions, is generally applicable to create liquid crystalline (LC) superlattices of polyamines. The structure and phase behavior of mixtures of an acid-modified discotic (**A-BTA**) with branched and linear poly(ethylene imine) (***b*-PEI** and ***l*-PEI**) and the linear organometallic polymer poly(ferrocenyl-(3-ammoniumpropyl)methylsilane) (**PFS**) were investigated. All mixtures were studied by polarizing optical microscopy, differential scanning calorimetry, infrared spectroscopy and X-ray scattering. Mixtures of **A-BTA** with ***b*-PEI** form a disordered oblique columnar LC phase featuring separate columnar microdomains of the polymer as a result of orthogonal hydrogen bonding and ionic interactions. Branching stabilizes the superlattice structure, but ***l*-PEI** with a molecular weight up to 250 kDa and **PFS** can also be incorporated in the nanostructured LC. The results show that the LC superlattice can serve as a general platform to achieve nanostructured functional materials by using various functional polymers.

1. Introduction

Many functional materials rely on a well-organized internal structure for their functional properties. In porous materials, for example, the structure and size of the pores determine the functionality of the material and allow these materials to be applied as membrane filters for size-selective separations ranging from the desalination of seawater (nanometer scale) to the clarification of beer and wine (micrometer scale).[1] Furthermore, materials with a well-ordered structure on a nanometer length scale are highly sought after for many application areas including organic solar cells,[2] nonvolatile memory devices,[3] and patterning templates.[4]

Liquid crystals (LCs) present an attractive option to design functional materials with a well-ordered internal structure and features smaller than 10 nm.[5] LCs are soft materials that combine self-assembled molecular order with a certain degree of mobility.[6,7] This unique combination yields well-organized materials that are able to respond to external stimuli (e.g., electrical, chemical, or mechanical).[8−11] Most notably by Tschierske and his co-workers, it has been shown that it is possible to design LC systems with very intricate structures by carefully balancing the anisotropic shape of the molecules, microsegregation between incompatible molecular segments, and specific intermolecular interactions.[12−16] There are several examples in the recent literature where these inherent properties of LCs and the ability to design structured LC phases have been exploited to obtain materials with functional properties such as nanoporosity[17,18] or ion conduction.[19−21]

In an earlier study we have shown that the second generation poly(propyleneimine) dendrimer (PPI-dendr) and the acid functionalized discotic **A-BTA** self-assemble to form a mixed columnar liquid crystalline (LC) phase through hydrogen bonding and ionic interactions that do not interfere with each other (orthogonal interactions).[22,23] In the LC phase, the PPI-dendr is confined to phase separated microdomains that form a well-ordered superlattice within the 2D columnar lattice of the discotic. A combination of phase separation between the strongly hydrophilic PPI-dendr and the hydrophobic discotic and a high contact area between the two components to allow for ionic complexation provides the main driving forces for the formation of a superlattice. The molecular structure of the second generation PPI-dendr makes it ideally suitable for such a mixed system, because it has a large number of amino groups for ionic complexation and its flexibility and branched nature permit efficient space filling.[24]

Although these perfectly branched dendrimers are well-defined and esthetically appealing molecules, they are inherently hard to synthesize and to purify compared to randomly branched analogues.[24] Therefore, it is worthwhile to explore the use of randomly branched polyamines for well-ordered mixed LC phases. Moreover, if availability of amino groups for complexation, hydrophilicity, and a flexible structure are indeed the most important prerequisites for superlattice formation, even linear polymers with a high amine content might be expected to self-assemble into a similar superlattice structure in the LC phase. Such systems are in the realm of what is sometimes referred to as ionic self-assembly (ISA).[25] In this field, the use of supramolecular ionic interactions between polymers and small molecules has been studied extensively to obtain nanostructured phases in both block copolymers and liquid crystals.[25,26] Poly(ethylene imine) (PEI) is an excellent polymer alternative for PPI-dendr, because it is structurally similar, has a high amine content and is commercially available as a linear and randomly branched polymer. Ionic complexes with smectic LC phases have been reported for PEI varying in molecular weight between 25 and 50 kDa.[27−31] More notably, Müllen and co-workers reported an example of ionic self-assembly between hydrophobically modified linear PEI (M_w ∼7 kDa) and an acid-functionalized hexabenzocoronene

*Corresponding author. E-mail: r.p.sijbesma@tue.nl.

Published on Web 01/19/2011

discotic.[32] In this system, however, the complexation does not result in a well-ordered superlattice structure in the LC phase and the polymer chains are randomly dispersed in the periphery of the discotics.

The use of polymers as a component in a columnar LC superlattice has great potential because the superlattice can either serve as a mold to structure the polymer component on a nanometer length scale or, alternatively, the LC phase itself can be functionalized in a supramolecular fashion by complexation of polymers with desirable properties. To fully realize this potential, it is important to confirm that the orthogonal self-assembly approach is more generally applicable to other, technologically relevant polymer classes. An example of such a class are derivatives of the main-chain organometallic polymer poly(ferrocenylsilane) (PFS). Because of its organometallic backbone PFS is redox active, conductive after partial oxidation and highly etch resistant.[33] These properties have led to considerable interest in PFS as etch resistant block in block copolymers and water-soluble PFS as an electroactive polyelectrolyte to form ultrathin multilayers via layer-by-layer deposition techniques.[34−36] Reports on LC materials with a PFS main-chain are scarce and only very recently a system based on supramolecular ionic interactions was reported.[37,38] In this study, a PFS polyelectrolyte was complexed with trisubstituted benzoic acid dendrons to yield smectic LC phases.

Here we report on the structure of mixed LC phases formed by orthogonal self-assembly between the previously reported acid-modified discotic (**A-BTA**, Scheme 1) and various polyamines to demonstrate that the orthogonal self-assembly approach to obtain well-ordered polymer containing LC phases is generally applicable for polyamines with varying molecular weight and chemical nature of the polymer backbone.

The molecular structures of the investigated amine-rich polymers are depicted in Scheme 1. Branched PEI (***b*-PEI**) has an approximate ratio of primary, secondary and tertiary amines of 1:2:1 and was singled out as a suitable polymeric analogue of PPI-dendr.[39] To address the issue of branching and molecular weight, the structures of complexes formed by **A-BTA** and three linear PEIs with molecular weights of 2.5, 25, and 250 kDa (***l*-PEI-low**, **-med**, and **-high**) were determined as well. Finally, a linear PFS derivative with one primary amino group per monomeric unit (poly(ferrocenyl(3-aminopropyl)methylsilane), **PFS**) was included in this study to investigate whether well-ordered mixed LC phases are also feasible for polymers with a completely different backbone structure.

The findings of this work will be presented and discussed in separate sections. First, the preparation of the mixtures and the synthesis of **PFS** will be treated. Next, the phase behavior and the LC structure are described for mixtures of **A-BTA** with both types of PEI and **PFS**, respectively. Finally, the results obtained for these three classes of polymers are compared and discussed.

2. Experimental Section

2.1. Materials. All solvents used were of AR quality or better and purchased from Biosolve or Sigma-Aldrich. Branched poly(ethylene imine) (***b*-PEI**, M_w = 2.0 kDa) was purchased as a 50 wt % aqueous solution from Sigma-Aldrich. Linear poly(ethylene imine) (***l*-PEI-low**, M_w = 2.5 kDa, ***l*-PEI-med**, M_w = 25 kDa, ***l*-PEI-high**, M_w = 250 kDa) was purchased from Polysciences, Inc. (Warrington, PA). Poly(ferrocenyl(3-ammoniumpropyl)methylsilane) (M_w = 940 kDa) was kindly provided by Dr. Mark Hempenius of the University of Twente.[40] The acid-modified BTA, **A-BTA** was synthesized as reported previously.[22] All chemicals were used as received.

2.2. Measurements. ^{1}H and ^{13}C NMR spectra were recorded at room temperature on a Varian Mercury NMR spectrometer (400 MHz for ^{1}H NMR, 100 MHz for ^{13}C NMR). Proton chemical shifts are reported in ppm downfield from tetramethylsilane ($Si(CH_3)_4$, TMS). Carbon chemical shifts are reported downfield from TMS using the resonance of deuterated chloroform ($CDCl_3$) as internal standard. DSC measurements were performed in hermetic T-zero aluminum sample pans using a TA Instruments Q2000−1037 DSC equipped with a RCS90 cooling accessory. The DSC experiments were conducted at a rate of 40 °C/min for all mixtures. The **A-BTA**/***b*-PEI** and the **A-BTA**/**PFS** mixtures were annealed at 100 °C for 15 min prior to the measurement. All transition temperatures and enthalpies were determined from the second heating run or the first heating run after annealing using Universal Analysis 2000 software (TA Instruments, USA). Variable temperature infrared (IR) spectra were recorded at an Excalibur TS 3000 MX from Biorad equipped with a Specac Golden Gate diamond ATR. All samples were allowed to equilibrate for 2 min at each temperature before recording the IR spectra, which were signal-averaged over 50 scans at a resolution of 2 cm^{-1}. The spectra for the **A-BTA**/linear PEI mixtures were recorded after fast cooling from the isotropic state. Polarizing optical microscopy studies were conducted using a Jeneval microscope equipped with crossed polarizers, a Linkam THMS 600 heating stage and a Polaroid DMC Ie CCD camera. The SAXS and WAXS measurements for all mixtures were performed on a Bruker AXS D8 Discover X-ray diffractometer with a Hi-Star 2D detector using Cu Kα radiation (λ = 1.54 Å) filtered by cross-coupled Göbbel mirrors at 40 kV and 40 mA. The sample−detector distance was set at 6 cm (WAXS) or 30 cm (SAXS). The sample holder was a home-built graphite oven. The temperature was controlled by a

Scheme 1. Molecular Structures of the Polyamines used for Orthogonal Self-Assembly with the Acid-Modified Discotic A-BTA

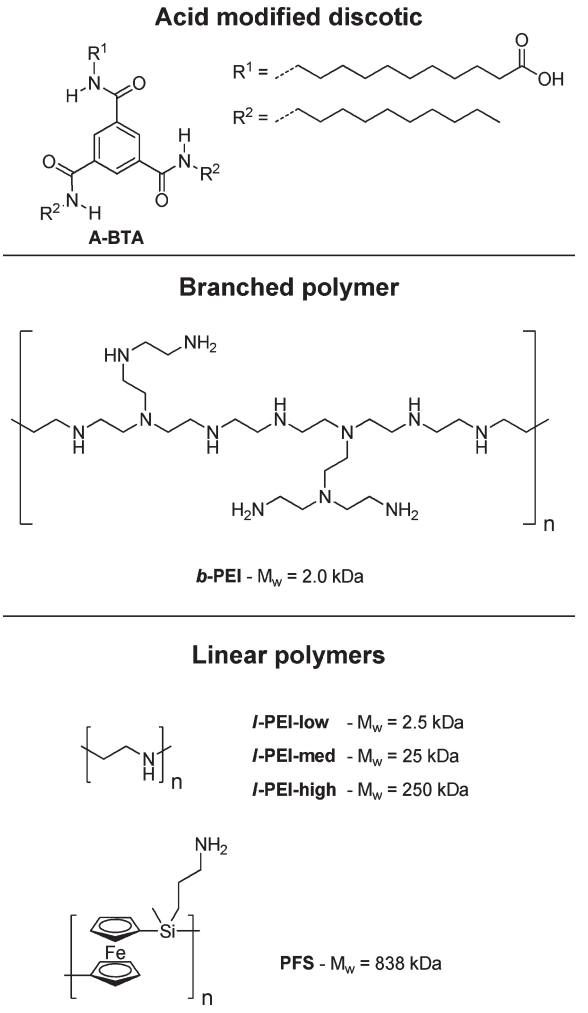

thermo-couple and a fast-response power supply (maximum heating rate 300 °C/min), which allowed a temperature range of 25−350 °C. Samples were prepared in a capillary-type glass cell with a diameter of 0.7 mm and a wall thickness of 0.01 mm (Mark-Röhrchen, Germany). The patterns for the **A-BTA**/***b*-PEI** and the **A-BTA**/**PFS** mixtures were collected after annealing the capillary containing the sample in the setup at a temperature of 100 °C for 5 min. The patterns for the **A-BTA**/linear PEI mixtures were recorded after fast (∼10 °C/min) cooling from the isotropic state. The SAXS and WAXS intensities were corrected by subtracting a background measured with an empty capillary cell. The Fit2D computer program (version 12.077) was used to integrate the two-dimensional scattering data.[41]

2.3. Preparation of Poly(ferrocenyl(3-amminopropyl)methylsilane) (PFS). The crude starting compound poly(ferrocenyl-(3-ammoniumpropyl)methylsilane) (100 mg) containing ∼15 wt % crown ether (dicyclohexano-18-crown-6) was dissolved in 50 mL deionized water. The solution was brought to a pH of 12 using a 0.1 M solution of NaOH and extracted three times with 50 mL of dichloromethane. The combined organic layers were dried over $MgSO_4$ and filtered. All solvent was evaporated from the filtrate and the remaining solid was redissolved in 8 mL of dichloromethane. This concentrated dichloromethane solution was precipitated in 50 mL of pentane. The resulting pentane solution was filtered and the residue was subsequently dried overnight under vacuum to yield the desired product as an orange solid (47 mg, 57%). ^{1}H NMR ($CDCl_3$): δ = 4.20−3.96 (m, 8H, Cp), 2.69 (t, 2H, CH_2NH_2), 1.50 (br, 2H, $SiCH_2CH_2$), 1.28 (br, 2H, NH_2), 0.88 (m, 2H, fcSiCH_2), 0.46 (s, 3H, fcSiCH_3). ^{13}C NMR ($CDCl_3$): δ = 73.6−70.6 (Cp), 45.8 (CH_2NH_2), 28.8 ($SiCH_2$-CH_2), 13.5 (fcSiCH_2), −3.0 (fcSiCH_3).

3. Results

3.1. Synthesis and Preparation of Mixtures. The acid-modified BTA, **A-BTA** was synthesized as reported previously.[22] All polyamines were procured from commercial sources except for **PFS**. This polymer was obtained as an orange-brown solid from poly(ferrocenyl(3-ammoniumpropyl)methylsilane)[42,40] after a basic extraction with dichloromethane and subsequent precipitation in pentane. The product was characterized by ^{1}H and ^{13}C NMR spectrometry. All mixtures were prepared by dissolving the appropriate amounts of **A-BTA** and polymer in a common solvent, evaporating the solvent and drying the mixture overnight under vacuum. The mixtures of **A-BTA** and PEI were dissolved in methanol and yielded flaky white solids after vacuum drying. The mixtures of **A-BTA** and **PFS** were obtained from a 1:1 methanol/dichloromethane mixture as flakey orange solids.

3.2. Mixtures of A-BTA with Branched and Linear PEI. Both ***b*-PEI** and linear PEI have a large number of amino groups available for complexation to **A-BTA**. However, the linear polymers exclusively contain secondary amines. Therefore, we decided to study the phase behavior of mixtures of **A-BTA** and PEI with a fixed weight content of the polymers rather than a specific acid/amine ratio. Our previous study showed that the Col_{ob} LC phase is formed in mixtures of **A-BTA** and PPI-dendr with a dendrimer content in the range of 10−20 wt %.[22] Consequently, mixing ratios of 14 and 18 wt % were used for all the polymers in the current study. The phase behavior and LC phase structure of these mixtures was studied by differential scanning calorimetry (DSC) and polarizing optical microscopy (POM). Additionally, small and wide angle X-ray scattering (SAXS and WAXS) and infrared (IR) spectroscopy were combined to elucidate the internal structure of LC phases.

3.2.1. Phase Behavior. Irrespective of the polymer and the mixing ratio, all mixtures of **A-BTA** and PEI were highly viscous and showed birefringent textures at temperatures above 80 °C indicating formation of a LC phase. Isotropization took place between 135 and 145 °C for the mixtures containing ***b*-PEI**, whereas the isotropization temperatures of the mixtures with linear PEI were markedly lower, around 120 °C. It proved impossible to grow textures with large domain sizes and distinct features by entering the LC phase from the isotropic liquid with a low cooling rate (1 °C/min).[43] We ascribe this observation to the formation of covalent amide bonds between **A-BTA** and the polyamines at temperatures above 100 °C.[22,44]

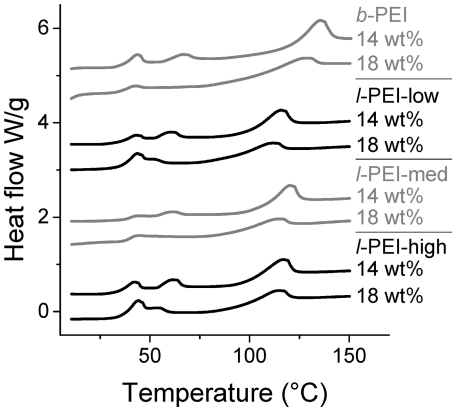

Figure 1. Differential scanning calorimetry traces (endothermic up, rate 40 °C/min) of all mixtures of **A-BTA** with branched and linear poly(ethylene imine) (low = 2.5 kDa, med = 25 kDa and high = 250 kDa). The individual traces are labeled on the right and grouped per polymer.

As a result of the amide formation, DSC experiments on the mixtures comprised of **A-BTA** and ***b*-PEI** showed considerable depression of the phase transition temperatures as well as broadening of the corresponding peaks in successive heating and cooling cycles, even at a high scan rate of 40 °C/min. In contrast, the DSC traces of consecutive heating runs measured for the mixtures containing linear PEI exhibited no noticeable depression of the transition temperatures. Apparently, the secondary amino groups in the linear polymers do not form amides on the time scale of the DSC experiments as opposed to the primary amines that are present in ***b*-PEI**. These observations reflect the higher reactivity of primary amines in amide formation and are consistent with results obtained in a study concerning cross-linking of acid-functionalized polymers in the melt with several difunctional amines.[45]

In view of the initial DSC results, the transition temperatures and enthalpies for the mixtures with ***b*-PEI** were determined from the first DSC heating run after annealing the samples at 100 °C for 15 min. For mixtures containing linear PEI, the second heating run at 40 °C/min was used to assess the phase transition parameters (Figure 1 and Table 1). Perhaps the most noticeable characteristic of the DSC traces recorded for the mixtures with PEI is that all transitions, especially at high temperature, are extremely broad. It is inherently hard to determine the onset temperatures of such broad transition peaks and, therefore, we also tabulated the peak temperature for the transition from the LC to the isotropic liquid. Another common feature of all the DSC traces is that the mixtures containing 14 wt % of PEI have slightly higher isotropization temperatures and the associated DSC transitions are much sharper in comparison to the corresponding mixtures containing 18 wt % of PEI. In agreement with the POM observations, both mixtures of **A-BTA** and ***b*-PEI** have a considerably higher clearing

Table 1. Phase Behavior of Mixtures of A-BTA with Branched and Linear Poly(ethylene imine)[d] and Poly(ferrocenyl-(3-aminopropyl)methylsilane)

			T, °C (ΔH, J/g)[b,c]				
polymer	wt %	acid/amine[a]					
***b*-PEI**	14	0.4	Cr	57 (2.0)	Col_{ob}	122/135 (10.6)	I
	18	0.3	Cr	35 (1.2)	Col_{ob}	104/126 (7.7)	I
***l*-PEI-low**	14	0.4	Cr	53 (1.6)	Col_{ob}	99/114 (8.7)	I
	18	0.3	Cr	37 (4.9)	Col_{ob}	89/108 (6.3)	I
***l*-PEI-med**	14	0.4	Cr	54 (1.0)	Col_{ob}	106/120 (8.6)	I
	18	0.3	Cr	38 (1.9)	Col_{ob}	91/111 (5.4)	
***l*-PEI-high**	14	0.4	Cr	54 (2.2)	Col_{ob}	98/115 (8.8)	I
	18	0.3	Cr	37 (6.4)	Col_{ob}	94/112 (6.7)	I
PFS	25	1.3			Col_{ob}	110/124 (6.4)	I
	30	1.0			Col_{ob}	111/123 (6.2)	I

[a] Molar ratio of acid groups in **A-BTA** to amino groups in the polymer (sum of primary, secondary and tertiary). [b] The onset temperatures and transition enthalpies of the isotropization and, if present, the last phase transitions preceding the isotropization are reported based on differential scanning calorimetry (40 °C/min). Temperatures were determined from the first heating run after annealing for the mixtures containing branched poly(ethylene imine) and poly(ferrocenyl(3-aminopropyl)-methylsilane), and the second heating run for the mixtures with linear poly(ethylene imine). The phases are identified by the following abbreviations: Cr = crystalline, Col_{ob} = disordered oblique columnar liquid crystal, and I = isotropic liquid. [c] For the transition to the isotropic liquid both the onset and top of the peak in differential scanning calorimetry are reported as follows: T_{onset}/T_{top}. [d] Key: low = 2.5 kDa, med = 25 kDa, and high = 250 kDa.

temperature than the mixtures with the linear polymer. The isotropization temperature of the mixture with 18 wt % ***b*-PEI** (top 126 °C) is comparable to pure **A-BTA** while the thermal stability of the LC phase in the 14 wt % mixture is higher (top 135 °C). The increase of the thermal stability of the LC phase for the mixtures of **A-BTA** with ***b*-PEI** is consistent with the formation of a mixed LC phase that is stabilized by ionic interactions.

Interestingly, the DSC traces for mixtures of **A-BTA** with ***l*-PEI-low**, **-med** and **-high** are practically equal for each mixing ratio. The transition temperatures from the LC phase to the isotropic state are around 115 and 120 °C (top) for the 18 and 14 wt % mixtures, respectively. These results show that the thermal stability of the LC phases in the mixtures is not increased with respect to pure **A-BTA** and that the molecular weight of the polymers does not influence the phase behavior notably. The reproducibility of the broad transitions in the DSC traces on successive heating cycles does indicate, however, that a single mixed LC phase is formed in the linear PEI mixture and that macroscopic phase separation does not take place.

3.2.2. Mesophase Structure: Col_{ob} Phases with a PEI Superlattice. To investigate whether **A-BTA** forms regularly stacked columns in the mixed LC phases with PEI, IR spectroscopy, and WAXS measurements were used. The IR spectra for all PEI mixtures at 100 °C in the LC phase are shown in Figure 2a. The IR spectra for the mixtures between **A-BTA** and ***b*-PEI** and the mixtures containing 14 wt % linear PEI show a fairly symmetric N−H stretch absorption band at ~3250 cm^{-1} and a sharp carbonyl stretch absorption around 1640 cm^{-1} originating from the amide groups in **A-BTA**. Several IR and X-ray diffraction studies have shown that BTAs form helical columnar structures through strong, 3-fold hydrogen bonding between the individual discotics and that the IR absorption bands at 3250 and 1640 cm^{-1} are indicative for this hydrogen bonding pattern.[22,46−49] The maxima of the main amide absorption bands are positioned at approximately the same wavenumbers for the 18 wt % mixtures containing linear PEI, but a shoulder is clearly visible on the high wavenumber side of both bands. The partial shift of these absorption bands indicates that the hydrogen bonding pattern along the columns is somewhat weaker than for the other mixtures and is consistent with the fact that 100 °C is rather close to the clearing temperature of the 18 wt % mixtures.

As can be expected based on these IR results, the WAXS patterns recorded at 100 °C exhibit an intense alkyl halo around 13 nm^{-1} and a weaker but clearly detectable maximum at 18 nm^{-1} corresponding to the characteristic disk−disk stacking distance of 0.35 nm for **A-BTA** (Figure 2b). The correlation length estimated from the latter peak for selected patterns in each series is in the order of 8−13 discotics.[50,51] These numbers are close to values found for pure **A-BTA** and demonstrate that the discotics possess only very short-range positional order along the column axis.

The 1700−1750 cm^{-1} region of the IR spectra also contains valuable information on the structure of these mixtures, because the carbonyl stretching vibration of uncomplexed acid groups gives rise to an absorption in this region. Whereas there is virtually no absorption in C=O stretch region of the free acid for the mixtures containing ***b*-PEI**, all mixtures between **A-BTA** and linear PEI exhibit considerable intensity in this part of the spectrum. In order to compare the extent of complexation quantitatively, the percentage of complexed carboxylic acid groups in **A-BTA** was calculated based on the intensity of the C=O stretch absorption at 1715 cm^{-1} relative to the amide band at 1640 cm^{-1}. As reference for the completely uncomplexed state we took the IR spectrum for pure **A-BTA** in the Col_{hd} phase at 100 °C.[52]

The estimated degree of acid complexation in all the mixtures containing 14 wt % of linear PEI is around 65% (Table 2). Because of the broadness of the amide band used for normalization, we did not calculate the extent of complexation for the 18 wt % mixtures of the linear polymers. Still, it can be expected that percentage of complexed acid groups falls in the same range as for the mixtures with a PEI content of 14 wt % based on the spectra. In contrast, around 80% of the acid groups are complexed in both ***b*-PEI** mixtures.

Evidently, the branched PEI allows for more efficient complexation in the mixed LC phase than the linear PEI. A difference in basicity between the secondary and tertiary amino groups and the primary amino groups, which are only present in the branched structures, cannot explain this fact, since the basicity of all three types of amines in solution is comparable for poly(imine) derivatives.[53] There are two other important differences between the linear and branched structures that influence their ability to form ionic complexes. First, the branched polymer is more preorganized to fill space evenly in the columnar microdomains of the superlattice, thus bringing the amino groups in close proximity to the acid groups in the periphery of the **A-BTA** columns. Second, the terminal amino groups in each branch have more conformational freedom to rearrange and form ionic complexes than the secondary amides in the main-chain of the linear polymer. In view of these arguments we ascribe the higher degree of complexation in the LC phases containing ***b*-PEI** primarily to these spatial factors.

The IR and WAXS results prove beyond doubt that all the investigated mixtures between **A-BTA** and PEI form columnar LC phases. The exact packing of these columns in a two-dimensional lattice was elucidated by SAXS measurements in the LC phase (100 °C).[54] The SAXS patterns for the mixtures containing ***b*-PEI** were measured after annealing at 100 °C. The two patterns are very similar and show the same peak positions and general features as the patterns

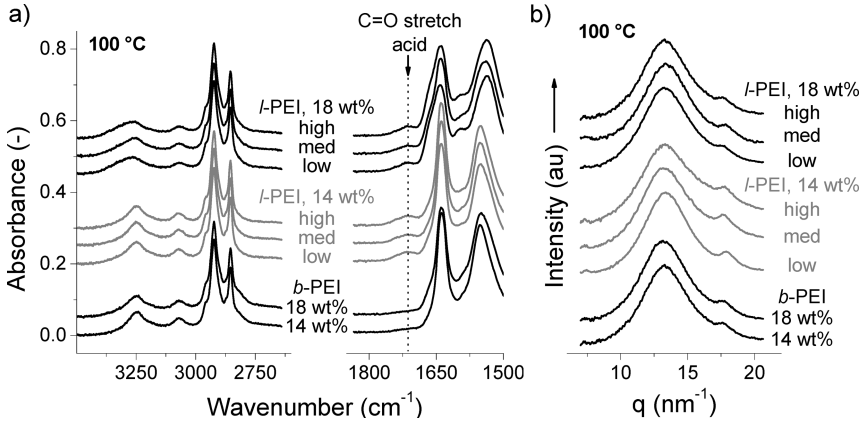

Figure 2. Infrared and X-ray scattering results for mixtures of **A-BTA** with branched and linear poly(ethylene imine) (low = 2.5 kDa, med = 25 kDa, and high = 250 kDa) at 100 °C. All data for linear poly(ethylene imine) was recorded after cooling from the isotropic liquid. (a) Infrared spectra (labeling in the middle of the spectra). The position of the C=O stretch absorbance band for free acid and acid dimers is indicated by the dotted line. (b) Wide angle X-ray scattering patterns (labeling on the right of the spectra).

obtained for the mixtures between **A-BTA** and PPI-dendr in the Col_{ob} phase in our previous study (Figure 3a).[22] The patterns were indexed with an oblique columnar lattice by supposing the same superlattice structure of ***b*-PEI** microdomains.[55] The unit cell dimensions and the calculated densities for the mixed LC phase are similar to the values found for the **A-BTA**/PPI-dendr system (Table 2). Therefore, we conclude that the mixed LC phase for the mixtures containing 14 and 18 wt % ***b*-PEI** can be characterized as an oblique columnar LC (Col_{ob}) with a well-defined superlattice of microphase segregated ***b*-PEI** domains.

In view of the earlier DSC results, SAXS experiments were performed on the mixtures containing ***l*-PEI-low**, **-med**, and **-high** after cooling the samples quickly from the isotropic state to 100 °C (Figure 3b). The SAXS patterns of all linear PEI mixtures show a sharp low-q reflection around 1.3 nm^{-1} and another strong maximum at ~3.8 nm^{-1} spaced relatively to the first as 1:3 in q-space. Unlike the patterns obtained for the Col_{ob} phase of the mixtures with ***b*-PEI**, the sharp midrange maximum is flanked on both sides by much weaker and broader maxima and no other reflections are detectable. The peak positions of these weaker maxima could not be reproduced by the same indexing procedure as applied previously. Apparently, a super structure is present in the LC phase of the linear PEI mixtures with approximately the same periodicity (~5 nm) but a different and less ordered structure than the Col_{ob} superlattice found for ***b*-PEI**.

To construct a structural model for the LC phase of the mixtures containing linear PEI, we first reconsidered the general structure of the original superlattice (Figure 4). The superlattice essentially consists of an oblique sublattice of **A-BTA** columns in which a number of lattice positions are periodically occupied by columns of the amine containing component. The exact 1:3 peak ratio between the low-q maximum and one of the midrange maxima in the SAXS patterns shows that the amine rich microdomains are located exclusively in one of the lattice planes of this sublattice with a periodicity that is precisely three times larger than the sublattice. Reversing this line of thought, one can construct a superlattice by first calculating the lattice parameters of the oblique sublattice from the three midrange SAXS peaks related to the positional order between single columns. Subsequently, this lattice can be expanded by adding lattice planes that correspond to the strongest SAXS reflection of the sublattice, indexed in this case as (110). Finally, the superlattice structure is fixed by adding polymer columns in every third (110) plane in an alternating fashion like in the original superlattice. The unit cell parameters of the superlattice constructed in this manner follow directly from the unit cell parameters of the smaller sublattice.

Table 2. Superlattice Unit Cell Parameters for Mixtures of A-BTA with Branched and Linear Poly(ethylene imine) (low = 2.5 kDa, med = 25 kDa and high = 250 kDa) and Poly(ferrocenyl-(3-aminopropyl)methylsilane) in the Col_{ob} Liquid Crystalline Phase

				lattice parameters[b,c]			
polymer	wt %	% compl.[a]	T, °C	*a*, nm	*b*, nm	γ, deg	ρ, g/mL[d]
***b*-PEI**	14	82	100	5.29	3.56	70.4	1.05
	18	80	100	5.22	3.58	70.0	1.11
***l*-PEI-low**	14	64	100	5.46	3.93	65.0	0.95
	18	-	100	5.40	3.93	66.3	1.00
***l*-PEI-med**	14	68	100	5.54	3.92	64.0	0.95
	18	-	100	5.51	3.89	65.4	1.00
***l*-PEI-high**	14	65	100	5.51	3.92	64.6	0.95
	18	-	100	5.48	3.92	65.3	1.00
PFS	25	60	100	5.11	3.73	67.2	1.21
	30	65	100	5.07	3.77	68.3	1.28

[a] The percentage of acid groups in **A-BTA** that is complexed to the polymer was estimated from the normalized intensity of the C=O stretch absorbance band of the remaining free acid at 1715 cm^{-1}. See main text for more details. [b] For full indexation of the branched poly(ethylene imine) patterns see Supporting Information. [c] The unit cell parameters for mixtures containing linear poly(ethylene imine) and poly(ferrocenyl-(3-aminopropyl)methylsilane) were calculated from the positions of the three midrange small-angle X-ray scattering peaks assuming an oblique sublattice. See main text for details. [d] Calculated from the unit cell parameters and the mixing ratio assuming 5 molecules **A-BTA** and all available polymer are present in the unit cell volume. See Supporting Information for a sample calculation.

The superlattice parameters were calculated via this approach from the three midrange SAXS maxima for all mixtures with linear PEI and are summarized in Table 2.[56] The lattice constants a (~5.5 nm) and b (~3.9 nm) do not change much over all mixtures. The monoclinic lattice angles are practically constant at 64−66°, only slightly lower than the ~70° angle for the original superlattice. The densities calculated based on the unit cell parameters are 0.95 and 1.00 g/mL for the mixtures containing 14 and 18 wt % of PEI, respectively.

Since there are only three peaks in the q-range around 3.8 nm^{-1} and an oblique columnar lattice is defined by three parameters (a, b, and lattice angle γ), the calculation procedure described above always yields an exact solution. As such, the structural model depicted in Figure 4 and the resulting unit cell parameters should be treated with some

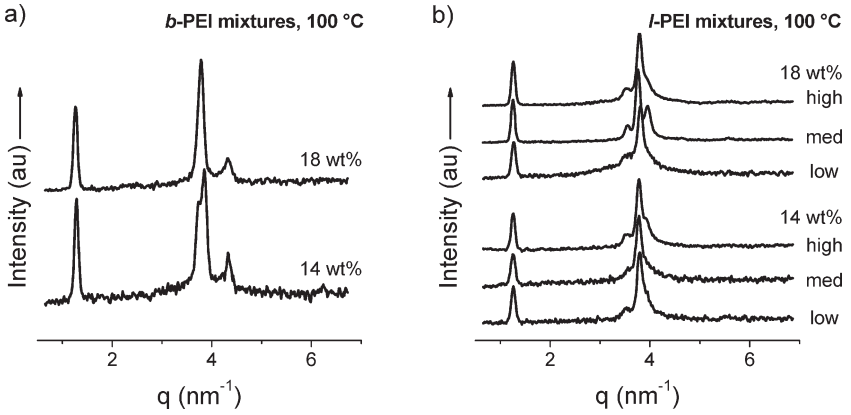

Figure 3. Integrated small-angle X-ray scattering patterns for the **A-BTA**/poly(ethylene imine) mixtures. (a) 14 and 18 wt % mixtures of **A-BTA** with branched poly(ethylene imine) at 100 °C. (b) Mixtures of **A-BTA** with linear poly(ethylene imine) at 100 °C (low = 2.5 kDa, med = 25 kDa, and high = 250 kDa; weight percentages indicated next to patterns).

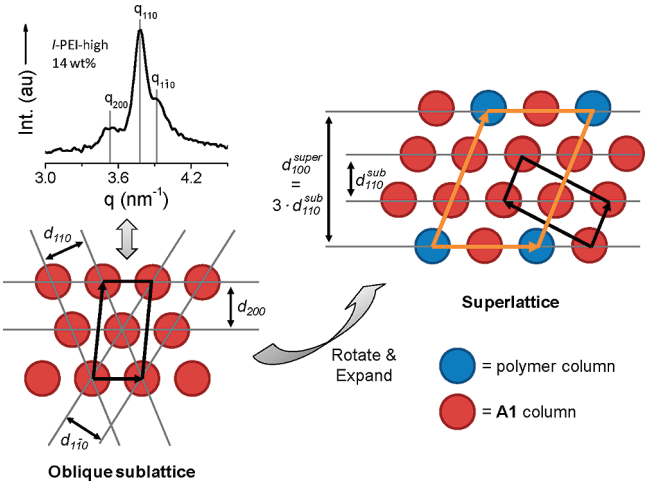

Figure 4. Pictorial representation showing the derivation of the proposed structural model for the superlattice for the mixtures of **A-BTA** with linear poly(ethylene imine) and poly(ferrocenyl(3-aminopropyl)methylsilane). The three midrange small-angle X-ray scattering peaks (example top left) are indexed with an oblique sublattice of **A-BTA** columns (bottom left, columns as red circles and unit cell in heavy black lines). Rotation followed by expansion perpendicular to the (110) direction and addition of polymer columns (blue circles) gives rise to the superlattice unit cell (right, unit cell in heavy orange lines).

caution. The calculated densities for the mixed LC phases provide supporting evidence for the proposed superlattice structure, because they fall in the expected range for organic compounds. In addition, the slightly lower densities as compared to the mixed LC phases for ***b*-PEI** are consistent with the lower degree of ionic complexation in the linear polymer mixtures as determined by IR spectroscopy. In summary, the structure in Figure 4 represents a proposed model which is in line with the available experimental data presented here and the results reported earlier for a similar system, but it leaves room for future refinements. Therefore, we tentatively assign an oblique columnar lattice (Col_{ob}) with a superlattice structure of microphase segregated polymer domains to all the LC phases formed by mixtures of **A-BTA** with linear PEI.

3.3. Mixtures of A-BTA with Linear PFS. The final polymer we studied for its LC phase behavior in mixtures with **A-BTA** is the organometallic linear polymer **PFS**. Because of its high iron content, these polymers are known to have a high density up to 1.4 g/mL.[57] Therefore, we expected that a significantly higher weight content of polymer would be needed to reach volume fractions of polymer comparable to the mixtures with PEI that were discussed previously. To allow for direct comparison with the other systems as well, we chose to investigate mixtures with a **PFS** content of 14, 18, 25, and 30 wt %. The mixing ratios of the latter two mixtures correspond to acid/amine stoichiometries of 1.3:1 and 1.0:1, respectively. The phase behavior and structure of the mixture of **A-BTA** with **PFS** mixtures were characterized with the same techniques used for the mixtures containing PEI.

3.3.1. Phase Behavior. The POM analysis of the mixtures between **A-BTA** and **PFS** revealed highly viscous phases with a birefringent texture up to temperatures of 130−140 °C. Above this temperature range, all mixtures became fluid and showed a black texture indicating a transition from a LC phase to the isotropic liquid. Since **PFS** solely contains primary amino groups, we performed the DSC experiments for the mixtures with a high scan rate of 40 °C/min after annealing at 100 °C (Figure 5a). The transition temperatures (onset and top) and the corresponding enthalpies for the 25 and 30 wt % mixtures were determined from the first heating run after annealing and are reported in Table 2. The DSC traces show that the clearing temperature and isotropization enthalpy of the LC phases is far higher for the two mixtures with the highest **PFS** content. The temperature of the transition to the isotropic state for the mixtures containing 25 and 30 wt % **PFS** is roughly equal (top 124 °C) and similar to the isotropization temperature of pure **A-BTA**. Interestingly, the mixtures with a **PFS** content of 25 and 30 wt % mixture do not show appreciable crystallization on the time scale of the DSC experiments. The absence of any crystallization peaks attributable to **A-BTA** shows that macroscopic phase separation does not take place and strongly indicates that both mixtures form a mixed LC phase held together by ionic interactions.

3.3.2. Mesophase Structure: a Col_{ob} Phase with a PFS Superlattice. To assess the hydrogen bonding pattern and the degree of acid complexation in the mixtures of **A-BTA** with PFS, the IR spectra of all four mixtures were measured in the LC phase at 100 °C (Figure 5b). The N−H stretch (not shown) and C=O absorption bands are located at wavenumbers that are characteristic for strong hydrogen bonding in regular columnar stacks of **A-BTA** (~3250 and ~1640 cm^{-1}, respectively). The region of the IR spectra between 1700 and 1750 cm^{-1} features two weak and overlapping peaks attributed to the C=O stretch absorption bands of uncomplexed carboxylic acid groups. The intensity of the C=O stretch bands in this region decreases sharply with increasing **PFS** content of the mixtures up to a ratio of 25 wt % and remains

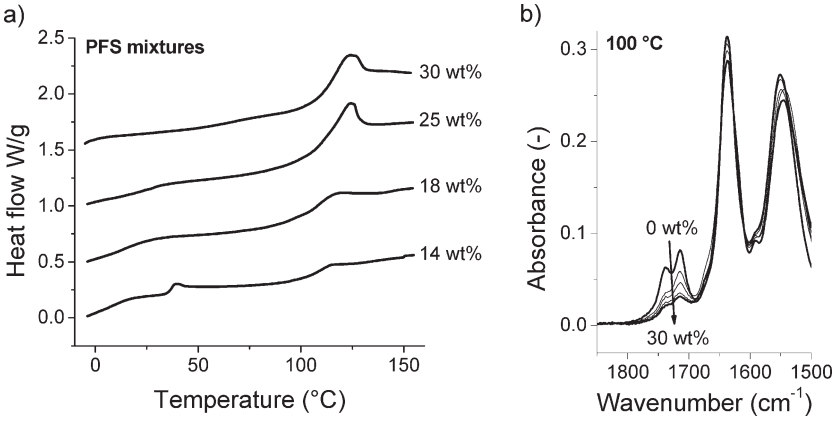

Figure 5. Differential scanning calorimetry and infrared results for mixtures of **A-BTA** with poly(ferrocenyl(3-aminopropyl)methylsilane). (a) Differential scanning calorimetry traces (endothermic up, rate 40 °C/min). The individual traces are labeled on the right. (b) Infrared spectra at 100 °C in the 1850−1500 cm^{-1} region for **A-BTA** and the mixtures containing 14, 18, 25, and 30 wt % poly(ferrocenyl(3-aminopropyl)methylsilane). The spectra for the 30 wt % mixture and **A-BTA** are plotted with a heavy line and the arrow indicates the observed trend with increasing content of poly(ferrocenyl(3-aminopropyl)methylsilane).

virtually constant in the 30 wt % mixture. Apparently, the added **PFS** can hardly participate in additional ionic bonding in this composition range despite the availability of free acid groups in the mixture. This trend becomes even clearer by looking at the extent of complexation estimated from the relative intensities of the uncomplexed acid absorption bands (selected values in Table 2). The percentage of complexed acid groups increases from 31% for the 14 wt % mixture to respective values of 60% and 65% for the two mixtures with the highest **PFS** content. These values are similar to the degree of complexation determined for the mixtures with linear PEI.

The internal structure of the LC phase in all four mixtures containing **PFS** was studied in more detail by X-ray scattering measurements (Figure 6). The WAXS patterns feature an intense and diffuse scattering maximum around 13−14 nm^{-1} characteristic for LC phases. At wider angles a very weak peak is observed corresponding to a distance of 0.35 nm and ascribed to the regular stacking of **A-BTA** in a columnar fashion. The latter wide-angle peak is much less clearly discernible than for pure **A-BTA** and the previously studied mixtures. Consequently, we were not able to make a reliable estimate of the correlation length along the column from these patterns. The low intensity of the peak related to interdisk stacking distance compared to the halo might indicate a lower degree of positional order in these LC phases, but might also be due simply to increased scattering in the halo region as a result of the high electron density in the organometallic main-chain of the polymer.

The SAXS patterns for all mixtures show a sharp peak in the low-q range at ∼1.3 nm^{-1} pointing to a periodic structure on a length scale of roughly 5 nm. The general intensity of the patterns recorded for the mixtures containing 14 and 18 wt % **PFS** is rather poor and the 3−5 nm^{-1} q-range is dominated by a very diffuse maximum with superimposed sharper reflections. Notably, the position of one of these sharp reflections in the 14 wt % mixture corresponds precisely to the hexagonal main peak of pure **A-BTA** at the same temperature. These aspects of the SAXS patterns are in accordance with the other experimental evidence from DSC as well as IR and strongly suggest that the **PFS** content in these mixtures is too low to form a single, well-defined mixed LC phase. As a consequence, we made no further attempts to index the SAXS patterns to a single columnar lattice.

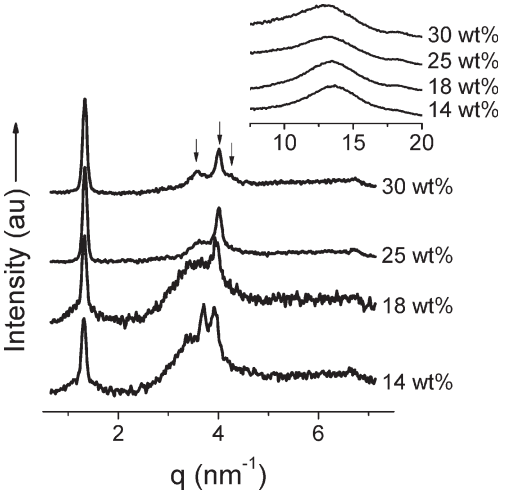

Figure 6. Small and wide (inset) angle X-ray scattering patterns for mixtures between **A-BTA** and poly(ferrocenyl(3-aminopropyl)methylsilane) in the liquid crystalline phase (14 wt % at 80 °C, 18−30 wt % at 100 °C). The arrows in the 30 wt % small angle pattern indicate the midrange scattering maxima used for indexation.

The two mixtures with the highest **PFS** content gave rise to far more intense SAXS patterns featuring a sharp peak at the same position as the mixture with lower mixing ratios and a set of three overlapping, yet clearly resolved maxima in the intermediate q-range. Strikingly, the low-q reflection in both patterns is far more intense than the set of peaks around 4 nm^{-1}. The position of the sharp central peak in this set relative to the strong low-q maximum is exactly 1:3 in q-space, whereas no obvious relation between the positions of the two more diffuse peaks could be identified. As such, the SAXS patterns for the two nearly stoichiometic mixtures of **A-BTA** with **PFS** have the same general features as the patterns recorded for the mixtures of **A-BTA** with linear PEI. Therefore, we again assumed an oblique sublattice of **A-BTA** columns and calculated the unit cell parameters for the superlattice by following the same strategy as depicted schematically in Figure 4. The results of this calculation for the 25 and 30 wt % mixtures are given in Table 2 together with the estimated densities of the mixed LC phases. The unit cell parameters are comparable to those reported previously for the PPI-dendr mixtures (∼5.1 nm and ∼3.7 nm) and the monoclinic lattice angle of the superlattice is nearly 70°.[22] As

expected based on the high density of **PFS**, the overall densities of the mixed LC phases are 1.2−1.3 g/mL, much higher than any of the other mixtures included in this study.

Finally, it is worth noting that the proposed superlattice structure accounts qualitatively for the high relative intensity of the low-q peak in the SAXS patterns of the mixtures with **PFS** in comparison to patterns recorded for analogous mixtures containing PEI. According to our model, the low-q peak originates from the ordered arrangement of microdomains of the polyamine within a sublattice of **A-BTA** columns. Since X-ray scattering relies on periodic differences in electron density, the intensity of the superlattice reflection is indeed expected to increase when the amine rich organic component in the superlattice is an organometallic polymer with a high electron density. Combining all structural evidence presented above, we conclude that the mixtures with a **PFS** content of 25 and 30 wt % form an oblique columnar LC phase (Col_{ob}) in which the organometallic polymer is organized in a relatively well-ordered superlattice.

4. Discussion

4.1. Columnar Superlattices with Nearly Equal Dimensions due to Orthogonal Interactions. In the literature there are several examples of ionic LC systems based on PPI-dendr and various PEI analogues.[27,29−31,58−61] These systems give rise to nematic, smectic, and sometimes columnar LC phases depending on the volume fraction of both components and the identity of the moieties used for the ionic complexation. In all these cases, the exact phase structure and the dimensions of its features are determined by the interplay between the structural properties of both components. What sets our system apart from these literature examples is the fact that a strong, directional hydrogen bonding interaction exists between the acid-modified discotics which acts orthogonal to the ionic self-assembly process. As a result, we observe Col_{ob} phases with a basic lattice spacing that is completely dictated by the molecular structure of the discotic acid **A-BTA** for all polymers, irrespective of branching, molecular weight and chemical nature of the backbone.

4.2. Branching Stabilizes the Superlattice. Compared to the mixtures containing ***b*-PEI** and the previously studied mixtures with PPI-dendr, the thermal stability of the LC phases for the mixtures of **A-BTA** with linear PEI and **PFS** is significantly lower and the degree of ionic complexation of the acids groups does not exceed 65%. Simultaneously, the lattice parameters of the LC superlattice are somewhat altered compared to the original superlattice and the 2D columnar lattice on a whole becomes less ordered as reflected by the lower number of observable diffraction maxima and their increased broadness. We ascribe the lower thermal stability of the LC phase and these structural changes to the fact that the linear polymers have to adopt a highly elongated, yet coiled conformation in the cylindrical microdomains of the superlattice to allow the amino groups in or close to the polymer backbone to interact with the acid groups of **A-BTA**. Such conformations are feasible for both polymers, since PEI is known to form helical structures in solution with a diameter in the same range as the columns in the mixed LC phases (0.8−1.6 nm) and the backbone of **PFS** is highly flexible because the iron atom in the ferrocene acts as "molecular ball-bearing".[33,62] Even so, the linear polymers can evidently not combine the overall cylindrical shape enforced by the superlattice structure with a high degree of complexation.

These results are in line with two systems reported by Ren and co-workers in which ionic LC phases formed by linear PEI were explicitly compared with branched PEI and with a linear polymer with primary amino groups connected to the backbone by a short spacer.[27,29] When wedge-shaped acids are used for complexation, the latter polymer is able to pack in a cylindrical shape and gives rise to a columnar LC phase, while linear PEI only yields a smectic LC phase. Furthermore, both studies showed that the ionic LC phases formed by linear PEI are thermally less stable than the corresponding phases of the polymers containing amino groups with more conformational freedom.

4.3. Linear Polymers: Size Does Not Matter. The most striking observation in our study of the mixtures of **A-BTA** with linear PEI is that there is virtually no difference in either phase behavior or phase structure between ***l*-PEI-low**, **-med**, and **-high**, even though the molecular weights of the polymers differ over 2 orders of magnitude. On the one hand, it seems logical that a clear size effect is absent in these linear polymers, because they simply fill a larger section of the columnar domains depending on their molecular weight. On the other hand, it is well-known that the average equilibrium conformation of flexible polymers in the melt can be described as a random coil with a diameter that scales with the square root of the molecular weight. Hence, longer linear polymers must also deform from their coiled equilibrium state to an increasingly stretched conformation in order to fill the columnar microdomains in the superlattice. Such stretching results in a loss of chain entropy and is accompanied by an increase in the free-energy of the system.

However, assuming that the PEI chains can be regarded as molten, ideal polymer chains in the LC phase, the free-energy penalty of confinement is roughly estimated to be in the order of 0.2 kJ/mol repeat unit.[63,64] This energy is about 2 orders of magnitude lower than interaction energy involved in the hydrogen bonded stacking of **A-BTA** (∼50 kJ/mol BTA) and the ionic complexation between the amino groups in the PEI backbone and the acid groups in **A-BTA** (50−250 kJ/mol ionic complex).[25,65] Thus, the free-energy penalty of confinement is negligible compared to the interaction energy the system gains by adopting the ordered superlattice structure, as is also reflected by the fact that the isotropization temperature of the LC phases does not decrease with increasing molecular weight of the PEI chains. The result is that flexible polymers with different lengths can be incorporated into the same ordered superlattice structure up to a molecular weight that is a factor 5−10 larger than reported so far for ionic LCs based on PEI.[27,29−31]

5. Conclusions

In this study, the structure and phase behavior of mixtures between an acid-modified discotic (**A-BTA**) and various polyamines have been investigated. Mixtures of **A-BTA** and ***b*-PEI** form a disordered oblique columnar LC phase with isotropization temperatures of 126−135 °C. The structure of these LC phases is identical to that reported in an earlier study for mixtures of **A-BTA** with PPI-dendr and features separate columnar microdomains of the polymer resulting from the orthogonal combination of hydrogen bonding in the columnar direction and ionic interaction in the plane perpendicular to the columns. The mixtures of **A-BTA** with linear PEI and the linear organometallic polymer **PFS** form disordered oblique columnar LC phases with a lower isotropization temperature of 100−120 °C. These LC phases display a superlattice structure of the polymer component as well, although the lattice is slightly less ordered than the superlattice in the mixtures containing ***b*-PEI** and the degree of ionic complexation between the two components is

lower. These results show that branching in the polymer stabilizes the structure of the LC superlattice.

An important implication of the superlattice structure is that a clear size effect is absent for the linear polymers allowing the incorporation of PEI with a molecular weight up to 250 kDa in LC phases with the same superlattice structure. The fact that also linear polymers with a completely different backbone such as **PFS** can be incorporated in a superlattice structure broadens the scope of our system. We envision that the LC superlattice can serve as a general platform to achieve nanostructured functional materials by using polymers for ionic complexation that provide, e.g., conductance, selective transport properties or etch resistance.

Acknowledgment. Ben Norder of the Technical University Delft is gratefully acknowledged for his help with the SAXS and WAXS measurements.

Supporting Information Available: POM images for **A-BTA**/***l*-PEI-med** mixture, IR spectra for ***l*-PEI-low** and **PFS**, two-dimensional SAXS and WAXS data for **A-BTA**/***l*-PEI-med** mixture, SAXS results for **A-BTA**/***b*-PEI** mixtures, sample calculation for the density of the mixed mesophases, and calculation of the free-energy of confinement ***l*-PEI**. This material is available free of charge via the Internet at http://pubs.acs.org.

References and Notes

(1) Mulder, M. *Basic Principles of Membrane Technology*; Kluwer Academic Publishers: Dordrecht, The Netherlands, 1996.
(2) Thompson, B. C.; Frechet, J. M. J. *Angew. Chem., Int. Ed.* **2008**, *47*, 58–77.
(3) Naber, R. C. G.; Asadi, K.; Blom, P. W. M.; de Leeuw, D. M.; de Boer, B. *Adv. Mater.* **2009**, *21*, 933–945.
(4) Bang, J.; Jeong, U.; Ryu, D. Y.; Russell, T. P.; Hawker, C. J. *Adv. Mater.* **2009**, *21*, 4769–4792.
(5) Kato, T.; Mizoshita, N.; Kishimoto, K. *Angew. Chem., Int. Ed.* **2006**, *45*, 38–68.
(6) Gray, G. W. In *Handbook of Liquid Crystals, Vol. 1, Fundamentals*; Demus, D., Goodby, J., Gray, G. W., Spiess, H.-W., Vill, V., Eds.; Wiley-VCH: Weinheim, Germany, 1998; p 1−16.
(7) Tschierske, C. *J. Mater. Chem.* **1998**, *8*, 1485–1508.
(8) Kouwer, P. H. J.; van den Berg, O.; Jager, W. F.; Mijs, W. J.; Picken, S. J. *Macromolecules* **2002**, *35*, 2576–2582.
(9) Sage, I. C. In *Handbook of Liquid Crystals, Vol. 1, Fundamentals*; Demus, D., Goodby, J., Gray, G. W., Spiess, H.-W., Vill, V., Eds.; Wiley-VCH: Weinheim, Germany, 1998; p 731−762.
(10) Suarez, M.; Lehn, J. M.; Zimmerman, S. C.; Skoulios, A.; Heinrich, B. *J. Am. Chem. Soc.* **1998**, *120*, 9526–9532.
(11) Tschierske, C. *J. Mater. Chem.* **2001**, *11*, 2647–2671.
(12) Chen, B.; Zeng, X. B.; Baumeister, U.; Ungar, G.; Tschierske, C. *Science* **2005**, *307*, 96–99.
(13) Cheng, X. H.; Prehm, M.; Das, M. K.; Kain, J.; Baumeister, U.; Diele, S.; Leine, D.; Blume, A.; Tschierske, C. *J. Am. Chem. Soc.* **2003**, *125*, 10977–10996.
(14) Kato, T. *Science* **2002**, *295*, 2414–2418.
(15) Tschierske, C. *Chem. Soc. Rev.* **2007**, *36*, 1930–1970.
(16) Ungar, G.; Liu, Y. S.; Zeng, X. B.; Percec, V.; Cho, W. D. *Science* **2003**, *299*, 1208–1211.
(17) Zhou, M. J.; Kidd, T. J.; Noble, R. D.; Gin, D. L. *Adv. Mater.* **2005**, *17*, 1850–1853.
(18) Zhou, M. J.; Nemade, P. R.; Lu, X. Y.; Zeng, X. H.; Hatakeyama, E. S.; Noble, R. D.; Gin, D. L. *J. Am. Chem. Soc.* **2007**, *129*, 9574–9575.
(19) Kato, T.; Yasuda, T.; Kamikawa, Y.; Yoshio, M. *Chem. Commun.* **2009**, 729–739.
(20) Yoshio, M.; Kagata, T.; Hoshino, K.; Mukai, T.; Ohno, H.; Kato, T. *J. Am. Chem. Soc.* **2006**, *128*, 5570–5577.
(21) Yoshio, M.; Mukai, T.; Ohno, H.; Kato, T. *J. Am. Chem. Soc.* **2004**, *126*, 994–995.
(22) Fitié, C. F. C.; Tomatsu, I.; Byelov, D.; de Jeu, W. H.; Sijbesma, R. P. *Chem. Mater.* **2008**, *20*, 2394–2404.
(23) Hofmeier, H.; Schubert, U. S. *Chem. Commun.* **2005**, 2423–2432.
(24) Bosman, A. W.; Janssen, H. M.; Meijer, E. W. *Chem. Rev.* **1999**, *99*, 1665–1688.
(25) Faul, C. F. J.; Antonietti, M. *Adv. Mater.* **2003**, *15*, 673–683.
(26) Hammond, M. R.; Mezzenga, R. *Soft Matter* **2008**, *4*, 952–961.
(27) Cheng, Z. Y.; Ren, B. Y.; Shan, H. Z.; Liu, X. X.; Tong, Z. *Macromolecules* **2008**, *41*, 2656–2662.
(28) Ren, B. Y.; Cheng, Z. Y.; Tong, Z.; Liu, X. X.; Wang, C. Y.; Zeng, F. *Macromolecules* **2005**, *38*, 5675–5680.
(29) Ren, B. Y.; Cheng, Z. Y.; Tong, Z.; Liu, X. X.; Wang, C. Y.; Zeng, F. *Macromolecules* **2006**, *39*, 6552–6557.
(30) Takahashi, T.; Kimura, T.; Sakurai, K. *Polymer* **1999**, *40*, 5939–5945.
(31) Zhou, S. R.; Shi, H. F.; Zhao, Y.; Jiang, S. C.; Lu, Y. L.; Cai, Y. L.; Wang, D. J.; Han, C. C.; Xu, D. F. *Macromol. Rapid Commun.* **2005**, *26*, 226–231.
(32) Thünemann, A. F.; Ruppelt, D.; Ito, S.; Müllen, K. *J. Mater. Chem.* **1999**, *9*, 1055–1057.
(33) Kulbaba, K.; Manners, I. *Macromol. Rapid Commun.* **2001**, *22*, 711–724.
(34) Bellas, V.; Rehahn, M. *Angew. Chem., Int. Ed.* **2007**, *46*, 5082–5104.
(35) Ma, Y. J.; Hempenius, M. A.; Vancso, G. J. *J. Inorg. Organomet. Polym. Mater.* **2007**, *17*, 3–18.
(36) Whittell, G. R.; Manners, I. *Adv. Mater.* **2007**, *19*, 3439–3468.
(37) Cheng, Z. Y.; Ren, B. Y.; Zhao, D. L.; Liu, X. X.; Tong, Z. *Macromolecules* **2009**, *42*, 2762–2766.
(38) Liu, X. H.; Bruce, D. W.; Manners, I. *Chem. Commun.* **1997**, 289–290.
(39) Odian, G. *Principles of Polymerization*, 4th ed.; John Wiley & Sons, Inc.: Hoboken, NJ, 2004.
(40) Hempenius, M. A.; Robins, N. S.; Lammertink, R. G. H.; Vancso, G. J. *Macromol. Rapid Commun.* **2001**, *22*, 30–33.
(41) Hammersley, A. P.; Svensson, S. O.; Hanfland, M.; Fitch, A. N.; Hausermann, D. *High Pressure Res.* **1996**, *14*, 235–248.
(42) Poly(ferrocenyl(3-ammoniumpropyl)methylsilane) was kindly provided by Dr. Mark Hempenius of the University of Twente and synthesized as described in ref 40.
(43) See Supporting Information for a representative set of POM images for the 14 wt % mixture of **A-BTA** with ***l*-PEI-med**.
(44) Martín-Rapún, R.; Marcos, M.; Omenat, A.; Barberá, J.; Romero, P.; Serrano, J. L. *J. Am. Chem. Soc.* **2005**, *127*, 7397–7403.
(45) Song, Z. Q.; Baker, W. E. *J. Polym. Sci., Part A: Polym. Chem.* **1992**, *30*, 1589–1600.
(46) Hanabusa, K.; Kawakami, A.; Kimura, M.; Shirai, H. *Chem. Lett.* **1997**, 191–192.
(47) van Gorp, J. J.; Vekemans, J. A. J. M.; Meijer, E. W. *J. Am. Chem. Soc.* **2002**, *124*, 14759–14769.
(48) Yasuda, Y.; Iishi, E.; Inada, H.; Shirota, Y. *Chem. Lett.* **1996**, 575–576.
(49) Lightfoot, M. P.; Mair, F. S.; Pritchard, R. G.; Warren, J. E. *Chem. Commun.* **1999**, 1945–1946.
(50) The correlation length (ξ) has been calculated by fitting the peak with a Lorentzian distribution function and using the Scherrer equation as reported in ref 51: $\xi = 0.89\,\lambda/(\omega \cos\theta)$, wherein λ is the wavelength of the X-rays, ω is the full width at half-maximum of the peak in radians, and θ is Bragg angle of the maximum of the peak.
(51) Kouwer, P. H. J.; Jager, W. F.; Mijs, W. J.; Picken, S. J. *J. Mater. Chem.* **2003**, *13*, 458–469.
(52) The main assumption in this calculation is that complete complexation results in zero absorption and, thus, that the other components in the mixture (PEI or **PFS**) do not contribute to the absorption in the 1750−1600 cm^{-1} region of the spectrum. As can be seen from the spectra of the pure polymers in the Supporting Information, this assumption is very reasonable.
(53) Koper, G. J. M.; van Genderen, M. H. P.; Elissen-Roman, C.; Baars, M. W. P. L.; Meijer, E. W.; Borkovec, M. *J. Am. Chem. Soc.* **1997**, *119*, 6512–6521.
(54) Two-dimensional X-ray scattering measurements on shear aligned samples showed that all small angle diffraction peaks split up in two opposing maxima that align in the same direction on the two-dimensional detector. Furthermore, the wide angle maximum related to the stacking of **A-BTA** splits up in two maxima perpendicular to the small angle diffraction peaks. These measurements confirm that all observed small angle diffraction peaks observed in the LC phase arise from order in a single plane perpendicular to the stacking direction of the **A-BTA** discotics. See Supporting

Information for a representative set of two-dimensional SAXS and WAXS data.
(55) See Supporting Information for full indexation
(56) The calculation requires a set of three equations relating the lattice plane spacings and the corresponding peak positions to be solved simultaneously. This system of equations was solved numerically in the programming language Python using an open-source library (see www.python.org and www.scipy.org).
(57) Temple, K.; Massey, J. A.; Chen, Z. H.; Vaidya, N.; Berenbaum, A.; Foster, M. D.; Manners, I. *J. Inorg. Organomet. Polym.* **1999**, *9*, 189–198.
(58) Cook, A. G.; Baumeister, U.; Tschierske, C. *J. Mater. Chem.* **2005**, *15*, 1708–1721.
(59) Marcos, M.; Alcala, R.; Barberá, J.; Romero, P.; Sanchez, C.; Serrano, J. L. *Chem. Mater.* **2008**, *20*, 5209–5217.
(60) Marcos, M.; Martín-Rapún, R.; Omenat, A.; Barberá, J.; Serrano, J. L. *Chem. Mater.* **2006**, *18*, 1206–1212.
(61) Tsiourvas, D.; Felekis, T.; Sideratou, Z.; Paleos, C. M. *Liq. Cryst.* **2004**, *31*, 739–744.
(62) Norman, A. I.; Fei, Y.; Ho, D. L.; Greer, S. C. *Macromolecules* **2007**, *40*, 2559–2567.
(63) See Supporting Information for the complete calculation.
(64) Rubinstein, M.; Colby, R. H. *Polymer Physics*; Oxford University Press: Oxford, U.K., 2003.
(65) Rochefort, A.; Bayard, E.; Hadj-Messaoud, S. *Adv. Mater.* **2007**, *19*, 1992–1995.